

Comparing satellite and ground-based observations of cloud occurrence over high southern latitudes

Cameron McErlich¹, Adrian McDonald^{1,2}, Alex Schuddeboom¹, and Israel Silber³

¹School of Physical and Chemical Sciences, University of Canterbury, Christchurch, New Zealand

²Gateway Antarctica, University of Canterbury, Christchurch, New Zealand

³Department of Meteorology and Atmospheric Science, Pennsylvania State University, University Park, PA, USA

Key Points:

- 2BCL5 and DARDAR cloud occurrences show large differences at low-levels globally, with the largest disparities at high southern latitudes
- Comparison with Antarctic ground observations tentatively suggests that this difference is likely due to false detections in DARDAR
- Some 2BCL5 and DARDAR cloud phase estimates do not adhere to physical constraints set by temperature from ECMWF-AUX or local radiosondes

Corresponding author: Cameron McErlich, cameron.mcerlich@pg.canterbury.ac.nz

This article has been accepted for publication and undergone full peer review but has not been through the copyediting, typesetting, pagination and proofreading process, which may lead to differences between this version and the [Version of Record](#). Please cite this article as [doi: 10.1029/2020JD033607](https://doi.org/10.1029/2020JD033607).

This article is protected by copyright. All rights reserved.

Abstract

The 2B-CLDCLASS-LIDAR R05 (2BCL5) and the raDAR/liDAR (DARDAR) satellite retrievals of cloud occurrence are compared as a function of altitude and latitude. The largest disparities are observed at low altitudes over high southern latitudes. These datasets are cross referenced to ground-based measurements from the Atmospheric Radiation Measurement (ARM) West Antarctic Radiation Experiment (AWARE) campaign at McMurdo Station, Antarctica. Compared to AWARE observations, both 2BCL5 and DARDAR underestimate cloud occurrence below 1.5 km, with 2BCL5 and DARDAR distinguishing roughly one third of cloud occurrences observed by AWARE at 0.5 km. While DARDAR identifies greater cloud occurrences than 2BCL5 below 1.5 km, cloud occurrence values for the two datasets have similar differences relative to ground-based measurements. Therefore, the DARDAR retrievals of greater cloud occurrence at low altitudes are likely due to a larger quantity of false positives associated with radar ground clutter or attenuated lidar retrievals. DARDAR cloud occurrences match better with AWARE than 2BCL5 above 5 km. However, the likely underestimation of ground-based measurements at higher altitudes suggests DARDAR may underestimate high level cloud occurrence. Finally, both datasets indicate the presence of liquid containing clouds at temperatures within the homogeneous freezing regime, despite the fact that the ECMWF-AUX dataset implemented in their processing clearly indicates temperatures below -38°C . Using AWARE radiosonde (ECMWF-AUX) temperature data, we find that 2BCL5 detects 13.3% (13.8%) of mixed phase clouds below -38°C , while DARDAR detects 5.7% (6.6%) of mixed phase and 1.1% (1.3%) of liquid phase clouds below -38°C .

1 Introduction

Clouds play a critical role in the Earth's energy balance. They can act to cool the surface by reflecting incoming solar radiation back into space or warm the surface by absorbing outgoing infrared radiation and radiating towards the surface (Marshall & Plumb, 2008). Although all clouds have an effect on the climate, clouds over the oceans are especially important due to the strong contrast in albedo between the sea surface and clouds. This means that the surface radiation budget over the ocean is more sensitive to cloud coverage than over land (Cess, 1990). These effects are greatest over the Southern Ocean which has an annual mean cloud coverage of around 80% - 90% (e.g., Kay et al., 2012; McCoy et al., 2014; Matus & L'ecuyer, 2017).

In this study, satellite measurements are used to evaluate cloud occurrence and cloud phase globally, with a focus over Southern Hemisphere high latitudes. Due to the limitations of satellite-based datasets in this region, a ground-based dataset is needed for independent examination of low level cloud. Unfortunately, ground-based measurements which vertically resolve cloud and cloud phase over the Southern Ocean are very rare due to the complicated logistics associated with collecting measurements from shipborne platforms. As such, ground-based measurements from the AWARE campaign over McMurdo Station in Antarctica are used as a representation of cloud at southern high latitudes. The AWARE dataset provides detailed cloud occurrence and phase measurements described in more detail in section 2.4, and is used for comparison with satellite-based measurements.

Comparisons between observations and models indicate significant shortwave radiation biases over the Southern Ocean with magnitudes of up to 30 Wm^{-2} (Trenberth & Fasullo, 2010). This shortwave bias induces warm sea surface temperature biases in climate simulations (Hyder et al., 2018), which limit the accuracy of models. The shortwave bias observed in the Southern Ocean has been identified as a contributory factor in a number of issues in models, such as the double-Intertropical Convergence Zone (e.g., Hwang & Frierson, 2013), errors in the meridional energy transport (e.g., Mason et al., 2015), biases in the position of the Southern Hemisphere storm track (e.g., Ceppi et al.,

2012) and the intensity of the Southern Hemisphere jet (e.g., Kay et al., 2016). Reduction of the shortwave bias over the Southern Ocean is thus critical to improving the simulation of climate at the Southern hemisphere mid- to high-latitudes.

Identifying the sources of these biases in climate models is an active and ongoing area of research. Though, Hyder et al. (2018) identified that 70% of the sea surface temperature bias in the Coupled Model Intercomparison Project Phase 5 (CMIP5) climate models relative to observations can be attributed to issues associated with the representation of clouds. Other work has shown that problems with the models include simulating too little cloud cover (e.g., Bodas-Salcedo et al., 2012; Schuddeboom et al., 2018; Kuma et al., 2020), excessive sunlight absorbed by the ocean surface (e.g., Trenberth & Fasullo, 2010; Hyder et al., 2018), a lack of clouds in the cold sectors of cyclones (e.g., Bodas-Salcedo et al., 2014), and a lack of reflective supercooled water clouds (e.g., Bodas-Salcedo et al., 2016; Kuma et al., 2020). Work has also shown that the bias over the Southern Ocean is not a single issue since there are different biases at higher and lower latitudes (Schuddeboom et al., 2019; Kuma et al., 2020).

Ice hydrometeors and water droplets have differing radiative properties and therefore reflect and absorb different levels of incoming shortwave radiation (e.g., Haynes et al., 2011; Scott & Lubin, 2014; Vergara-Temprado et al., 2018). Previous work has identified that supercooled clouds are very common over the Southern Ocean and Antarctica (e.g., Chubb et al., 2013; Jolly et al., 2018; Listowski et al., 2018; Morrison et al., 2011) and are potentially a major contributor to known model biases (e.g., Bodas-Salcedo et al., 2016; Kay et al., 2016; Kuma et al., 2020). In particular, Bodas-Salcedo et al. (2016) identified that clouds with supercooled tops contribute between 27 and 38% to the total reflected solar radiation over the Southern Ocean, and suggested that climate models poorly simulate these clouds. Models that overestimate the amount of ice cloud will produce a positive shortwave radiation bias, due to changes in the cloud albedo. As the introduction of ice into supercooled liquid clouds also causes the rapid growth of ice crystal at the expense of the liquid droplets (Vergara-Temprado et al., 2018), a minor error representing cloud phase can have large impacts.

Boundary layer observations by satellite instruments are limited by the presence of an almost continuous cloud cover in the Southern Ocean which acts to obscure low-level clouds. Unfortunately, measurements from satellites using passive instruments such as the Moderate Resolution Imaging Spectroradiometer (MODIS; Salomonson et al., 2002) and the International Satellite Cloud Climatology Project (ISCCP; Rossow & Schiffer, 1999) can only observe radiation scattered or emitted from the cloud top of optically thick clouds. Therefore, one can accurately identify the cloud properties at the top of the cloud with passive instruments, but cannot resolve the full vertical profile of clouds in most cases. Instead, active instruments such as those aboard the CloudSat and Cloud-Aerosol Lidar and Infrared Pathfinder Satellite Observation (CALIPSO) satellites need to be used to investigate cloud vertical structure.

Due to the limitations of satellite observations in the lower troposphere, ground based measurements from sub-Antarctic and Antarctic sites can provide essential information about cloud vertical structure. Surface based lidar instruments can detect layers of liquid water in the boundary layer, but similar to space-borne lidars, their signal becomes attenuated by optically thick cloud. Ground based radars can penetrate through these optically thick clouds, but miss a portion of the optically and geometrically thin high-altitude ice clouds due to a lack of sensitivity (Protat et al., 2006, 2010). In this study, we compare two sets of satellite observations with ground-based observations made at an Antarctic site to gain insight into the level of underestimation of low-level cloud occurrence across high Southern latitudes.

2 Datasets and Methods

2.1 The CloudSat and CALIPSO satellites

The satellite datasets used in this study are merged products created from CloudSat and CALIPSO observations. Launched together in April 2006, these satellites follow each other closely in orbit, initially as part of the A-Train constellation of satellites occupying a low Earth orbit (Stephens et al., 2002) and their measurements can be used to investigate the vertical distribution and properties of cloud. A partial equipment failure in 2017 forced CloudSat into a lower orbit to preserve the longevity of the instrument. CALIPSO was also moved into this lower orbit so that the two could continue to be used in conjunction. CloudSat has operated in daylight-only mode since 2011 due to a battery anomaly, which has inhibited nighttime measurements and reduced the quality of measurements collected during the sunlit portion of its orbit (Nayak, 2012).

The Cloud Profiling Radar (CPR), a 94 GHz radar that uses 3.3 μ s pulses, is the primary instrument onboard the CloudSat satellite (Stephens et al., 2002). The main instrument onboard CALIPSO is the Cloud-Aerosol Lidar with Orthogonal Polarization (CALIOP) (Winker et al., 2007). CALIOP transmits two laser pulses at wavelengths of 1064 nm and 532 nm simultaneously and measures backscatter data at two polarisations. The backscattered signal is used to derive vertical profiles of aerosol and cloud properties, and the ratio of backscatter at the two wavelengths is used to discriminate between clouds and aerosols as well as to determine the composition of cloud (Winker et al., 2009; Z. Liu, 2009). The lidar depolarisation ratio can also be used to estimate the phase of scattering hydrometeors as either ice or liquid water (Sassen, 1991; Hu et al., 2009). CloudSat's CPR, has a horizontal footprint of 1.4 km x 1.8 km, and vertical resolution of 485 m up to a height of 25km (Stephens et al., 2008). CloudSat uses the strength of the signal reflected off hydrometeors to determine cloud vertical structure. However, CloudSat is affected by surface clutter below approximately 1.2 km (cf. Marchand et al., 2008; Tanelli et al., 2008) while the CALIPSO lidar signal is attenuated by passing through optically thick cloud.

2.2 The 2BCL5 data product

In this study we use the 2B-CLDCLASS-LIDAR R05 (2BCL5) dataset generated by combining measurements from CloudSat and CALIPSO to determine the vertical distribution of clouds, cloud phase, and cloud type (Sassen et al., 2008; Wang, 2019). Because of the different horizontal and vertical resolutions of the two instruments, data from several CALIOP footprints are matched to the larger CPR footprints. 2BCL5 has resolutions of 60 m in the vertical and 1 km in the horizontal. Unfortunately, the CALIOP linear depolarisation ratio measurement is limited by the attenuation of the lidar signal through thick clouds, so the 2BCL5 data product does not use this data to derive cloud phase. Instead, differences between the number concentration, vertical distribution and radiative properties of ice particles and water droplets are used to generate a temperature dependent radar reflectivity (Z_e) threshold (cf. Zhang et al., 2010). This Z_e threshold is used alongside the integrated attenuated lidar backscattering coefficient and cloud base and top temperatures to distinguish between ice, liquid, and mixed phases cloudy air volumes (see Wang, 2019). The 2BCL5 product uses ancillary data from the ECMWF-AUX (Partain, 2007) product to provide temperature data.

Using 2BCL5 observations from 2016, cloud occurrence is derived as a function of altitude for different cloud phases. The vertical extent of the cloud is determined using the CloudLayerBase and CloudLayerTop fields. Using these heights, vertical bins are then created in between the cloud base and cloud top at a resolution of 60m. Cloud occurrence is assigned to the bins using the CloudFraction field. This process is repeated for each separate cloud layer in the 2BCL5 detection. Further partitioning using information about the three phase classification options produces separate cloud masks for each

168 phase. Profiles are summed and then normalised by using the total number of measure-
169 ments.

170 **2.3 The DARDAR data product**

171 The second satellite dataset used in this study is the raDAR/liDAR (DARDAR)
172 dataset. DARDAR is also a merged product derived from CloudSat and CALIPSO mea-
173 surements (Delanoë & Hogan, 2010), and uses ancillary temperature information from
174 ECMWF-AUX. It therefore uses identical inputs to the 2BCL5 dataset. DARDAR v.2.11
175 (Ceccaldi et al., 2013) was also obtained for 2016, chosen to coincide with ground based
176 measurements also used in this study. DARDAR provides vertically resolved profiles of
177 cloud phase, identifying ice, mixed and liquid phase clouds. The phase determination
178 algorithm also requires thermodynamic variables taken from the ECMWF-AUX prod-
179 uct. Similarly to 2BCL5, CALIPSO footprints are matched to CloudSat resolution for
180 merging. Likewise, DARDAR has resolutions of 60 m in the vertical and 1 km in the hor-
181 izontal. DARDAR cloud phase classification processes are detailed in Delanoë and Hogan
182 (2010), but were updated in Ceccaldi et al. (2013) upon the release of the DARDAR v2
183 product.

184 DARDAR cloud measurements are grouped into a categorization mask that sep-
185 arates cloud into different categories. While it includes cloud features such as supercooled
186 water and ice hydrometeors, it also contains features such as aerosols and ground clut-
187 ter not relevant to this study. To produce vertical profiles of cloud occurrence, the ap-
188 propriate features (such as supercooled and water cloud) are selected to partition the
189 data into clouds masks associated with the different phases. As for 2BCL5, these cloud
190 masks are combined to generate cloud occurrences. Cloud occurrence profiles for each
191 phase are merged by summing the cloud occurrence across each vertical level and nor-
192 malised using the total number of measurements.

193 **2.4 The AWARE dataset**

194 The ground-based observations obtained during the 2016 Atmospheric Radiation
195 Measurement (ARM) West Antarctic Radiation Experiment (AWARE) field campaign
196 in Antarctica are used in this study. The AWARE campaign took place between Novem-
197 ber 2015 and January 2017 (Lubin et al., 2020), primarily at McMurdo Station (77.85°S,
198 166.72°E), and provides an unprecedented cloud and radiation dataset in this region (Lubin
199 et al., 2020). In this study, we focus on AWARE measurements of cloud occurrence, cloud
200 phase, and temperature.

201 The AWARE dataset used in this study includes hourly cloud masks generated from
202 Ka-Band ARM Zenith Radar (KAZR; Widener et al., 2012) and the High Spectral Res-
203 olution Lidar (HSRL; Eloranta, 2005) measurements from McMurdo Station. These mea-
204 surements are then gridded onto a fixed 7.5 m and 10 s vertically- and temporally-spaced
205 grid, as detailed in Silber et al. (2018). This dataset spans from 1 January to 31 Decem-
206 ber 2016. KAZR was operated in two interleaved modes; a moderate sensitivity mode
207 was used to detect upper-tropospheric clouds and a general mode used to detect lower-
208 tropospheric clouds. We also use radiosonde soundings of temperature gathered twice
209 daily and linearly gridded to the vertical grid of the hourly cloud masks (cf. Silber et
210 al., 2018). AWARE observations include a significant quantity of cloud observations whose
211 phase could not be identified, particularly at high altitudes, due to the attenuation of
212 the lidar signal.

213 Both the KAZR and HSRL datasets have a high uptime, with more than 97% to-
214 tal data availability during 2016 (Silber et al., 2018). However, specific hours with low
215 data availability might still cause a potential sampling bias in our analysis. Therefore,

we set a hourly KAZR and HSRL data availability threshold of 75% (45 min) for cloud profiles to be considered in this analysis, this effectively rejects 2.3% of the AWARE dataset.

2.5 Combined Satellite and Ground-based Processing

To inter-compare the AWARE, 2BCL5 and DARDAR datasets, all of the observational datasets need to be constrained both spatially and temporally. First the satellite data was masked so that only observations falling within a 5 degree by 5 degree latitude/longitude box centered on McMurdo Station were used. The AWARE data was also masked so that only measurements within 3 hours before or after a CloudSat/CALIPSO overpass are considered. All measurements from CloudSat/CALIPSO and the AWARE datasets include both cloud and precipitation masks. Only the months of January, October, November and December had significant quantities of coincident satellite and ground based observations. Observations were also available for the months of March and September, however they did not include enough passes to provide sufficient statistics for evaluation. The passes used for comparison with the AWARE dataset were further filtered to only include passes where both 2BCL5 and DARDAR have concurrent observations, which gave a total of 180 passes.

The observational region (5 degree by 5 degree latitude/longitude box centered on McMurdo Station) was identified so that it would be large enough to contain a considerable number of satellite passes, but small enough to exclude the Trans-Antarctic mountains (See McErlich (2020), section 4.1.2). The temporal coincidence was chosen to ensure that the different instruments would observe the same synoptic weather patterns. Work by Coggins et al. (2014) used the k-means clustering technique to produce a synoptic climatology of the Ross Sea and Ross Ice Shelf regions and identified the characteristic time periods of each synoptic state in the region persisted for between 13 and 20 hours. A later study by Jolly et al. (2018) used this synoptic climatology to quantify the vertical distribution of cloud occurrence, phase, and type over the Ross Ice Shelf and southern Ross Sea, which encompasses McMurdo Station. They found large differences between the synoptic regimes relative to seasonal variation for the cloud occurrence as a function of altitude (see also Silber et al., 2019). An additional study in which examined Eulerian cloud persistence using the AWARE data was also carried out by Silber et al. (2018). They investigated the persistence of all cloud layers, as well as those that necessarily contain liquid water, and reported a mean cloud persistence between 5 and 10 hours depending on the month. However, liquid-containing cloud layers have a much shorter mean persistence of 2.7 hours and 54% do not last for more than an hour. A temporal threshold of 1 hour from either side of the closest AWARE measurement during a satellite overpass (a 3 hour window in total) was selected based on these studies.

3 Results

3.1 Global distribution of satellite-based cloud occurrences

Before using the ground-based AWARE observations, the 2BCL5 and DARDAR datasets are directly compared. Figure 1 shows the latitudinal cloud occurrence as a function of altitude for the 2BCL5 dataset during 2016. While only 2016 is examined the mean values used in this analysis are representative of other years (analysis not shown). Figure 1 displays cloud occurrence for the ice, mixed and liquid cloud phases, as well as the combined total alongside temperature isotherms generated using monthly averages of ECMWF-AUX temperature profiles (Partain, 2007). The 0 °C isotherm identifies the location where liquid hydrometeors will begin to freeze into ice phase cloud; at higher temperatures only liquid phase cloud should generally be present. The -38 °C isotherm was chosen to represent the edge of the homogeneous freezing regime (Lamb & Verlinde, 2011). Below this temperature any supercooled water present in the cloud will freeze into ice crystals, such that only ice phase clouds will be present. Between the two thresholds there will be a

266 combination of ice and supercooled water, so liquid, ice and mixed phase clouds can be
 267 present.

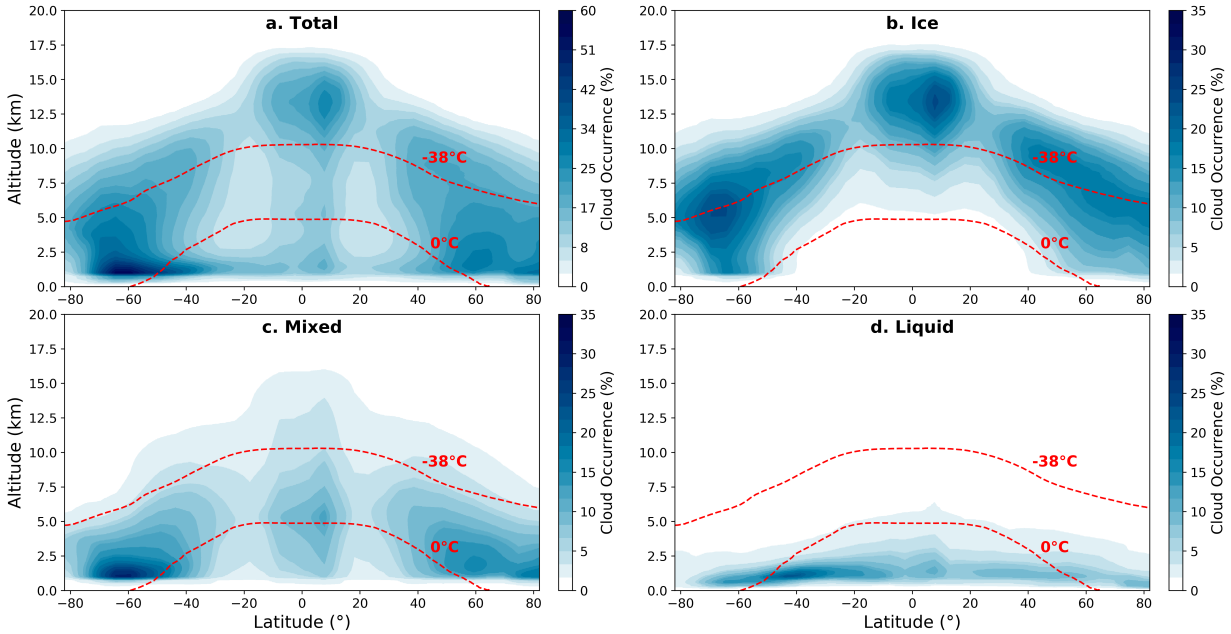


Figure 1. Latitudinal distribution of cloud occurrence as a function of altitude for the (a) total amount of cloud occurrence, as well as the (b) ice, (c) mixed and (d) liquid phases derived from the 2BCL5 observations from 2016. The dashed lines indicate isotherms of constant temperature generated using ECMWF-AUX temperature information.

268 A notable feature of Figure 1 is a sharp reduction in the amount of cloud detected
 269 by 2BCL5 below an altitude of 1 km, present across all latitudes and phases. This high-
 270 lights limitations in the 2BCL5 dataset at detecting cloud below this altitude. Figure
 271 1b shows that ice phase cloud is absent in the tropical and subtropical regions below 5
 272 km, where temperatures are higher, although there are some samples at temperatures
 273 below the 0 °C isotherm where ice phase clouds are present. Figure 1c shows that mixed
 274 phase clouds are generally present at altitudes above the -38 °C isotherm and below the
 275 0 °C isotherm. Figure 1d shows liquid phase cloud at temperatures lower than 0 °C,
 276 which is plausible due to the presence of supercooled water. However as the 2BCL5 liquid clas-
 277 sification does not distinguish supercooled water as a separate classification, further anal-
 278 ysis assessing the quality of liquid phase partitioning cannot be done. The reduction of
 279 cloud observed by 2BCL5 below 1 km has particular implications over the Southern Ocean
 280 (50 °S - 75 °S) where low level cloud occurrence peaks, but where it is also considered
 281 to be underestimated in models (Bodas-Salcedo et al., 2012; Schuddeboom et al., 2018;
 282 Kuma et al., 2020).

283 Figure 2 shows the differences between DARDAR and 2BCL5 cloud occurrence rates
 284 as a function of latitude and altitude. As 2BCL5 and the DARDAR datasets are gener-
 285 ated from the same satellite data, any differences between these two datasets is a re-
 286 sult of the dataset processing. Figure 2a shows that overall 2BCL5 detects more cloud
 287 than DARDAR, except below 1 km where DARDAR identifies greater cloud occurrences.
 288 These differences are greatest near 65 °S, over the Southern Ocean and Antarctic region.
 289 When the total cloud occurrence is partitioned into the ice, mixed, and liquid cloud phases
 290 further differences between the datasets become apparent. Figure 2c shows that 2BCL5

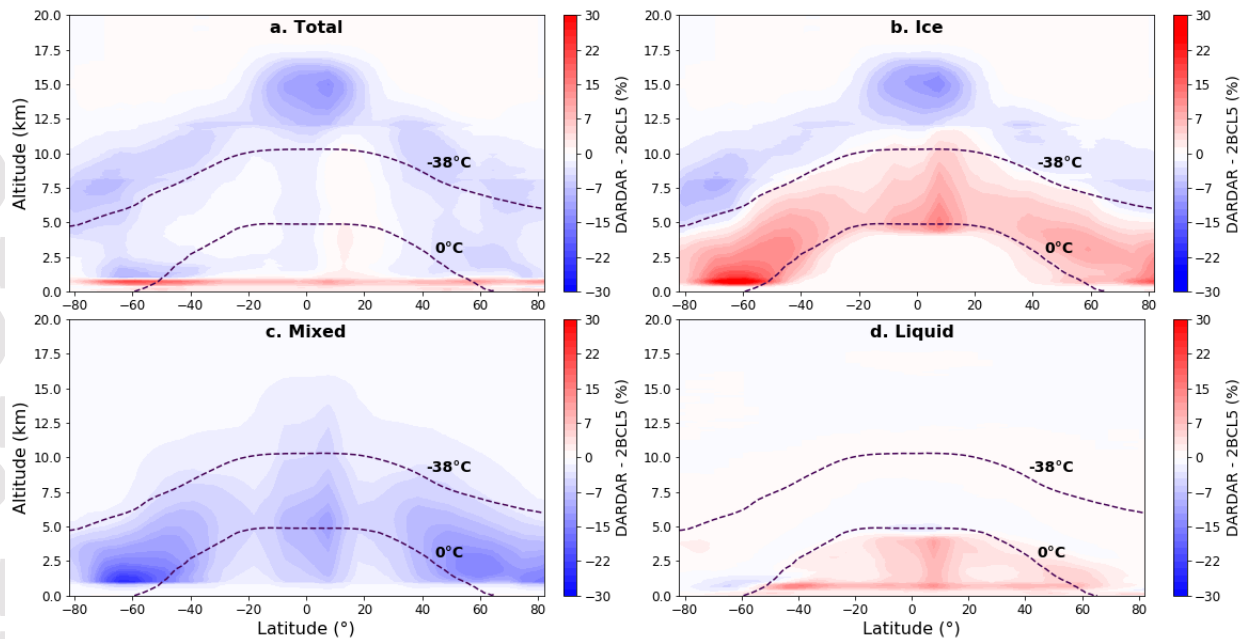


Figure 2. Differences in cloud occurrence between DARDAR and 2BCL5 during 2016, broken into (a) the total amount of cloud occurrence and (b) ice, (c) mixed and (d) liquid phase components. A positive value indicates DARDAR has a greater cloud occurrence than the 2BCL5 product. The dashed lines indicate isotherms of constant temperature generated using ECMWF-AUX temperature information.

291 always detects a larger occurrence of mixed phase cloud than the DARDAR dataset, with
 292 an absolute difference up to 25% over the Southern Ocean maximum at approximately
 293 65S. DARDAR classifies these clouds as either ice or liquid depending on temperature,
 294 as can be seen in Figure 2b and Figure 2d. Figure 2b also shows a clear regional separation
 295 of the 2BCL5 and DARDAR data. The difference between these regions match
 296 well with the position of the -38°C isotherm, with DARDAR detecting more ice phase
 297 cloud at altitudes corresponding to temperatures in between the 0 and -38°C isotherms
 298 than the 2BCL5 dataset. Previous work comparing and assessing algorithms for detecting
 299 phase over the Southern Ocean, Huang et al. (2012) found that between 40S - 65S
 300 DARDAR is dominated by ice phase cloud. This matches the results in Figure 2 where
 301 DARDAR displays predominantly ice phase cloud with little mixed phase cloud. Figure
 302 2a shows only small differences in 2BCL5 and DARDAR cloud occurrence between
 303 these isotherms, indicating the differences must be a result of the phase identification
 304 algorithms. Figure 2d shows DARDAR detects more liquid phase clouds below the 0°C
 305 isotherm, with 2BCL5 classifying the cloud in this region as mixed phase cloud (Figure
 306 2c). Some portion of the observations classified as mixed phase cloud by the 2BCL5 algorithm
 307 also lie outside the 0°C and -38°C isotherms, which disagrees with the physical
 308 limitations on cloud phase set by the temperature constraints defined by the ECMWF-
 309 AUX model output.

3.2 Cloud occurrence as a function of altitude

311 The greatest differences in cloud occurrence between 2BCL5 and DARDAR lie in
 312 their representation of low-level clouds over the Southern Ocean. This provides a strong
 313 motivation for a more detailed investigation of this region which includes the usage of

314 ground based radar/lidar data. The cloud occurrence rate over McMurdo Station as a
 315 function of altitude for each of the AWARE, 2BCL5 and DARDAR datasets is shown
 316 in Figure 3. These profiles are shown individually for January, October, November and
 317 December. Cloud profiles for each satellite overpass are averaged over the month and
 318 split into their constituent phases. The filled curves in Figure 3 represent the DARDAR
 319 (a-d) and 2BCL5 (e-h) cloud occurrences and the dashed curves represent the AWARE
 320 observations. The cloud occurrences from 2BCL5 in Figure 3 can be compared with pre-
 321 vious work investigating cloud phase using four years of 2BCL4 data over the Ross Sea
 322 and Ross Ice Shelf detailed in Jolly et al. (2018). In general, there is good agreement
 323 with respect to the mean cloud occurrence profiles obtained in this study and the results
 324 for the 2BCL4 dataset used in Jolly et al. (2018). This suggests that the 2016 2BCL5
 325 data is statistically representative of the long-term cloud patterns observed in this re-
 326 gion.

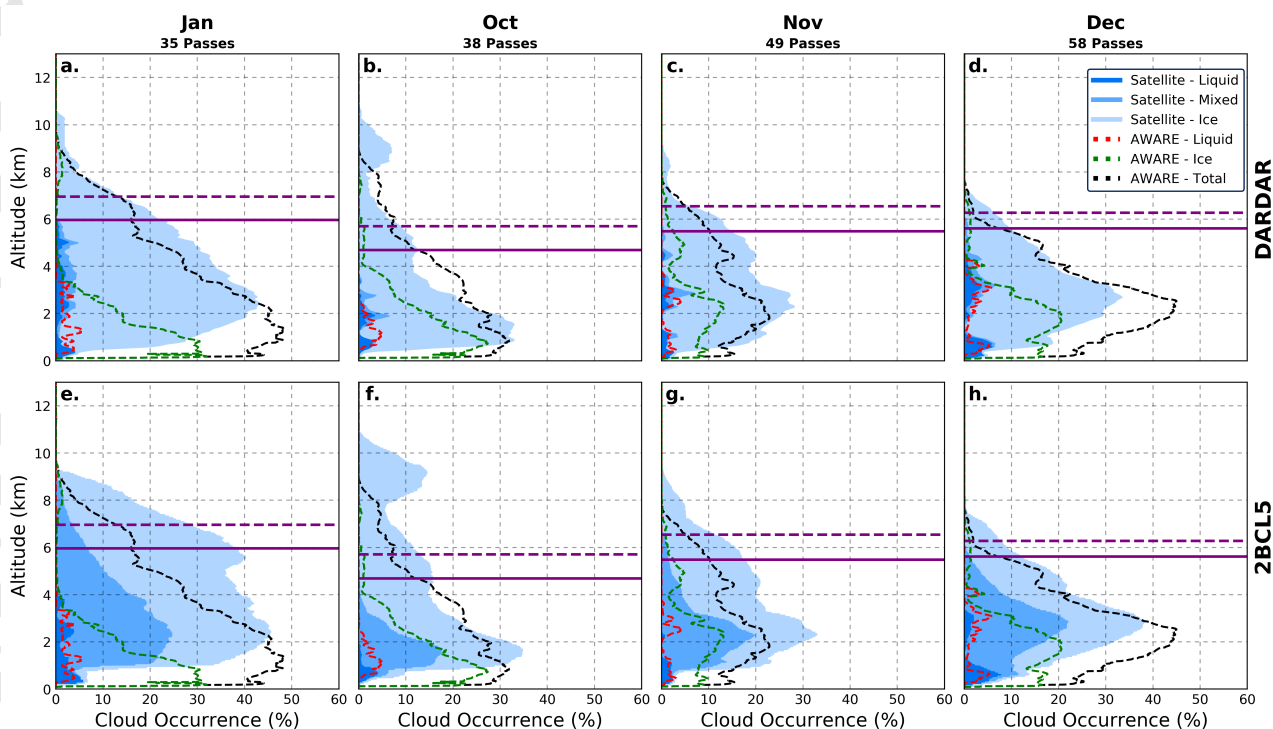


Figure 3. Mean vertical profiles of cloud occurrence for different cloud phases derived from observations over McMurdo Station during 2016. The dashed lines represent the AWARE cloud occurrence and the filled curves represent coincident DARDAR (a - d) and 2BCL5 (e - h) cloud occurrences. The number of passes are annotated at the top of the figure. The purple lines represents the mean (solid) and maximum (dashed) altitudes of the $-38\text{ }^{\circ}\text{C}$ isotherm across all passes, derived from twice-daily radiosonde observations.

327 The AWARE cloud profiles show limited amounts of liquid phase clouds. These clouds
 328 are confined to the bottom 4 km of the atmosphere except during December (Figure 3d)
 329 where liquid phase clouds occur up to an altitude of 4.5 km. Liquid phase clouds have
 330 a maximum occurrence rate of 5%, with no obvious vertical structure across the months
 331 examined. The AWARE ice cloud phase extends much higher than the liquid phase cloud,
 332 but shows reduced frequency above an altitude of 4 km. This reduction is balanced by
 333 an increase in cloud occurrence in the 'unknown' phase category. Ice phase cloud peaks
 334 at an altitude below 1 km during January and October (Figure 3a-b), but peaks at 2–

335 2.5 km during November and December (Figure 3c-d). The unknown phase clouds in the
336 AWARE dataset dominate the cloud occurrence above altitudes of 4 km in all months,
337 due to the extinction of the lidar signal preventing classification of the cloud phase. The
338 altitudes at which the clouds are most commonly classified as unknown phase are the
339 same altitudes at which ice phase clouds dominate the satellite datasets. This highlights
340 that the unknown phase class predominantly represents ice (volume-wise) as also noted
341 by (cf. Silber et al., 2018). Previous work detailed in (Jolly et al., 2018) also supports
342 this interpretation.

343 Figure 3a-d shows that the DARDAR cloud occurrence vertical profiles have liquid-
344 containing clouds that extend up to an altitude of 6 km and a maximum occurrence of
345 just over 5%. Mixed phase clouds are detected in the same altitude range as liquid phase
346 clouds, but have a lower occurrence. The majority of DARDAR-detected clouds are clas-
347 sified as ice phase and extend to an altitude of 10 km. The cloud occurrence maxima for
348 ice phase cloud generally occurs between 2 and 3 km, but is observed at a lower altitude
349 during October (Figure 3b). Below this maxima, DARDAR cloud occurrence falls rapidly
350 to values less than 10% below 1 km. No liquid or mixed phase cloud is identified in the
351 DARDAR dataset above the monthly maximum level of the -38°C isotherm, indicat-
352 ing DARDAR is conforming to liquid and mixed phase temperature constraints correctly.

353 Figure 3e-h identify vertical profiles of cloud occurrence for the 2BCL5 data prod-
354 uct. These shows liquid phase cloud occurrences of up to 10% between the surface and
355 5 km, with the maximum occurrence between 0.3 and 1 km. Liquid phase cloud occur-
356 rence tends to drop off rapidly at altitudes above the maxima, although this drop is not
357 as rapid in the summer months (December and January). The maximum occurrence of
358 mixed phase cloud is consistent over all the examined months, falling between 2 and 3
359 km. October (Figure 3f) has the lowest quantity of mixed phase clouds compared to other
360 months and shows no mixed phase cloud occurrence above 4 km. This is likely a reflec-
361 tion of the low altitude of the -38°C isotherm in this month. Interestingly, the other months
362 show mixed phase clouds up to 6.5km, meaning that clouds are observed above the max-
363 imum level of the -38°C temperature isotherm derived from radiosondes. In particular,
364 in January mixed phase clouds are present up 9 km which is much higher than the 7 km
365 maximum of the -38°C isotherm (Figure 3e). This shows clear limitations in how the
366 2BCL5 mixed phase cloud occurrence is determined with respect to temperature. The
367 representation of cloud phase in the DARDAR dataset is better confined by the -38°C
368 isotherm than 2BCL5.

369 Comparison of the monthly mean cloud occurrence profiles from the two satellite
370 datasets in the vicinity of McMurdo station shows that the 2BCL5 dataset has system-
371 atically higher cloud occurrences than the DARDAR dataset, except below 1 km where
372 DARDAR has a higher occurrence of cloud than the 2BCL5 dataset. This matches with
373 the global result displayed in Figure 2. Although these datasets differ, the relationship
374 between cloud occurrence and altitude is similar in both datasets in general.

375 Comparison of the cloud occurrence profiles show that at a higher altitude the AWARE
376 dataset likely underestimates cloud compared to the satellites datasets and at lower alti-
377 tudes there is an underestimation of 2BCL5 and DARDAR cloud occurrences compared
378 to AWARE. The satellite-based datasets are unable to detect a high number of clouds
379 below 1 km, and conversely, the ground-based measurements are unable to detect as many
380 clouds as 2BCL5 above 4km. As AWARE observations are often attenuated at higher
381 altitudes, the good match with DARDAR observed might suggest that DARDAR is ac-
382 tually underestimating cloud occurrence. Therefore, we postulate that differences between
383 2BCL5 and DARDAR above 1 km are a result of an underestimation in DARDAR cloud
384 occurrence. The discrepancy between the satellite- and ground-based peak in cloud oc-
385 currence as a function of altitude indicates that neither can obtain a complete picture
386 of the vertical profile of cloud occurrence in this region.

387 Examination of the liquid phase cloud profiles shows a number of differences be-
 388 tween the three datasets. Liquid phase cloud profiles for AWARE match well with the
 389 DARDAR profiles during November (Figure 3c) and December (Figure 3d), but match
 390 more poorly in January and October (Figure 3a and b). It is likely that November and
 391 December were dominated by optically-thin clouds that both datasets capture, while Jan-
 392 uary and October were dominated by frequent frontal systems, that resulted in the large
 393 discrepancies between the satellite and ground-based measurements. Overall, neither the
 394 2BCL5 or DARDAR datasets consistently agree with the liquid phase cloud reported by
 395 the AWARE dataset. Given the known weaknesses in the satellite datasets at detecting
 396 low-level cloud, this is expected. Ice-only phase cloud profiles are difficult to compare,
 397 due to both a lack of a reliable mixed phase cloud classification in the AWARE dataset
 398 and discrepancies in the definition of ice-only clouds in the satellite datasets.

399 3.3 2BCL5 and DARDAR cloud detections compared to AWARE

400 Figure 3 shows that both 2BCL5 and DARDAR underestimate cloud occurrence
 401 at low altitudes compared to AWARE observations, but is limited as it does not provide
 402 a direct comparison of individual profiles. To compare the individual profiles between
 403 the datasets, the frequency of cloud detections between 2BCL5, DARDAR, and AWARE
 404 for each pass over McMurdo Station during 2016 is examined. Cloud detections for the
 405 space-borne (S) and ground-based (G) observations are separated into three categories:

- 406 1. Where both the space-borne and ground-based observations identify cloud de-
 407 tectations (The intersection of both the space-borne and ground-based observations
 408 is identified, $S \cap G$).
- 409 2. Where only the ground-based observations has a cloud detection (The intersec-
 410 tion of the ground-based observations with the complement of the space-borne
 411 observations is identified, $S^c \cap G$).
- 412 3. Where only the space-borne observations has a cloud detection (The intersection
 413 of the space-borne observations with the complement of the ground-based obser-
 414 vations is identified, $S \cap G^c$).

415 Figure 4 shows a comparison of the detection frequency between 2BCL5 and AWARE
 416 (a, d, g) and DARDAR and AWARE (b, e, h) for the three previously defined categories.
 417 This allows us to assess if one or both the space-borne and ground-based instruments
 418 detect cloud at a particular altitude. The detection frequency is defined as the propor-
 419 tion of the time across all passes where the underlying conditions between the two sets
 420 are satisfied. Differences in the detection frequency for each category are displayed in
 421 Figure 4 (c, f, i) to highlight the discrepancies between 2BCL5 and DARDAR.

422 Figure 4 a shows that above 1 km AWARE observations detect clouds that are not
 423 identified by the 2BCL5 dataset approximately 10% of the time. Below 1 km the AWARE
 424 dataset detects a greater amount of clouds than observed by 2BCL5, with a maximum
 425 difference of 53%. As such, 2BCL5 is unable to accurately detect low altitude clouds re-
 426 lative to ground-based observations. Conversely, Figure 4d shows that the 2BCL5 has ob-
 427 servations undetected by AWARE 10% - 20% from near the surface to roughly 6.5 km.
 428 While cloud detections observed only by 2BCL5 at higher altitudes might be expected,
 429 it is surprising that 2BCL5 detects clouds that are not observed by AWARE at lower al-
 430 titudes.

431 These results suggest either limitations in the AWARE dataset, differences between
 432 the satellite footprint and ground observations, or a potential issue with 2BCL5 falsely
 433 identifying clutter in the radar and/or lidar signals as cloud detections. Figure 4g shows
 434 that below 9 km the frequency of AWARE and 2BCL5 both detecting cloud increases
 435 until it peaks at 42% near 2 km after which a sharp decrease is observed.

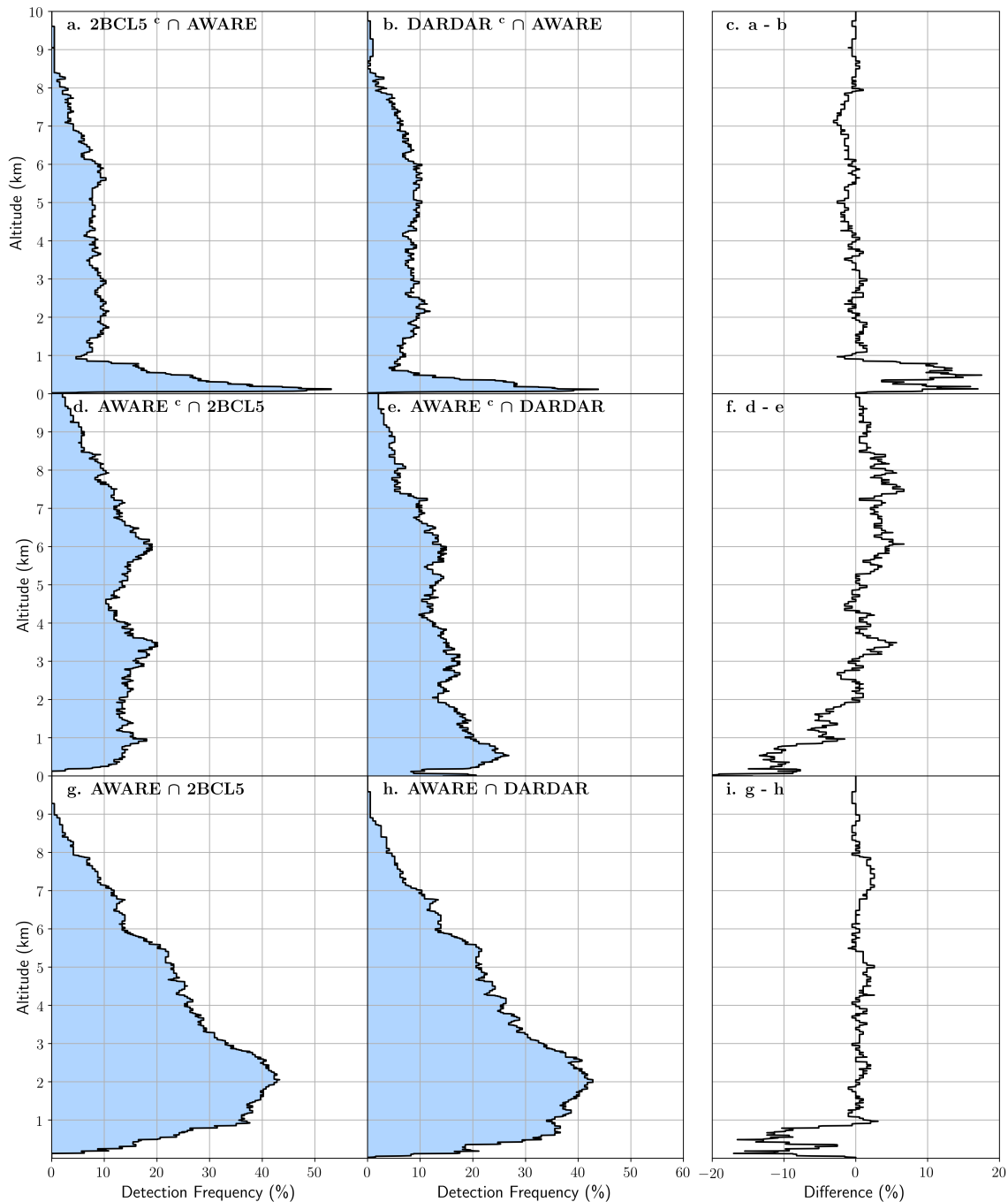


Figure 4. Detection frequency as a function of altitude for (a, d, g) 2BCL5 and AWARE and (b, e, h) DARDAR and AWARE showing where only the ground-based (a, b), space-borne (d, e) or both (g, h) datasets have cloud detections. Differences in the detection frequency for each categorisation are also displayed (c, f, i) to highlight the anomaly between 2BCL5 and DARDAR.

436 Figure 4b compares the DARDAR and AWARE datasets and shows that above 1
 437 km AWARE detects clouds unobserved in the DARDAR dataset approximately 10% of
 438 the time. Below 0.8 km the frequency where only AWARE observes a cloud detection
 439 rises to a peak of 44%. This likely indicates that both of the satellite datasets are un-

440 able to accurately observe clouds below 1 km. Figure 4e shows that between 1 and 7 km
441 DARDAR detects clouds unobserved by AWARE roughly 10% - 20% of the time. Above
442 7 km the frequency reduces to below 10% as detections become sparse. Interestingly, be-
443 low 1 km the frequency increases to 25% of the DARDAR overpasses identifying a cloud
444 unobserved by AWARE. This either suggest instrumental limitations in the AWARE dataset
445 or issues with DARDAR where false positives in the radar/lidar signals are detected. The
446 latter hypothesis is more likely given the known weaknesses in the satellite datasets. Fig-
447 ure 4h shows that similar to 2BCL5, the frequency of both DARDAR and AWARE ob-
448 serving cloud increases at lower altitudes, peaking at 42% at an altitude of 2 km, followed
449 by a decrease at lower altitudes.

450 While similar overall, both 2BCL5 and DARDAR display some differences in how
451 their cloud detections match with AWARE. Above 1 km, DARDAR and 2BCL5 show
452 good agreement, while below 1 km there is a large difference between the two datasets.
453 Figure 4c shows that below 1 km cases where only AWARE detects a cloud is 10% - 15%
454 greater for 2BCL5 than DARDAR. This is mirrored by Figure 4i where below 1km, DAR-
455 DAR observes a greater amount of cloud detections than 2BCL5, which are also observed
456 by AWARE. This result suggests that DARDAR agrees better with AWARE than 2BCL5
457 below 1 km, while the two have comparable detectability elsewhere. However, this could
458 be a result of DARDAR having greater cloud occurrences than 2BCL5 below 1 km, rather
459 than an improved match with AWARE. Figure 4e shows that below 1 km, DARDAR has
460 a greater amount of cloud detections where AWARE does not observe any cloud rela-
461 tive to 2BCL5. This probably indicates that DARDAR is classifying noise in the radar/lidar
462 signals close to the ground as clouds, resulting in a 10% - 15% larger false positive rate
463 than 2BCL5.

464 3.4 Ratios between satellite and ground-based detected cloud occur- 465 rences

466 The 180 satellite overpasses in which 2BCL5, DARDAR, and AWARE all detected
467 clouds were examined and spatially and temporally colocated atmospheric profile from
468 the different datasets were compared. Figure 5a and b show the ratio of 2BCL5 and DAR-
469 DAR cloud occurrence to the AWARE cloud occurrence for each co-location, respectively.
470 Figure 5 a and b also show the median value at each altitude for both 2BCL5/AWARE
471 (red) and DARDAR/AWARE (black). The ratio between 2BCL5 and DARDAR is dis-
472 played in Figure 5c with the median curve illustrated in blue.

473 Figure 5a shows that the median ratio of cloud occurrence between 2BCL5 and AWARE
474 match well between 1.5 and 4.5 km, with relative differences less than 10%. However,
475 there is a large spread of values at this altitude range, which indicates that while it is
476 common for the two datasets to detect similar cloud profile structures, this is not always
477 the case. Below 1.5 km the median ratio shows that 2BCL5 underestimates cloud oc-
478 currence compared to the AWARE dataset. This ratio decreases to a local minimum of
479 0.24 at 0.8 km, corresponding to an underestimation in 2BCL5, identifying that 2BCL5
480 only observes 24% of the cloud occurrence relative to the AWARE observations. Below
481 0.8km the detectability of 2BCL5 improves slightly, with 2BCL5 observing 37% of AWARE
482 cloud occurrence at 0.5 km, before steadily decreasing below 0.25 km. Above 4.5 km the
483 two datasets also disagree, but with AWARE likely underestimating compared to 2BCL5.
484 As the altitude increases the median ratio fluctuates up to an altitude of around 7.5 km
485 and then steadily increases until AWARE observes between 37%–61% of cloud observed
486 by 2BCL5. Above this altitude there is little consistency as the AWARE instruments have
487 difficulties in detecting clouds at this altitude.

488 Figure 5b also shows agreement between DARDAR and AWARE. Between 3 and
489 5 km there is good agreement (within 10%). Extending this range to between 1.5 and
490 6 km there is poorer agreement with differences of up to 20%. Similar to the 2BCL5 dataset,

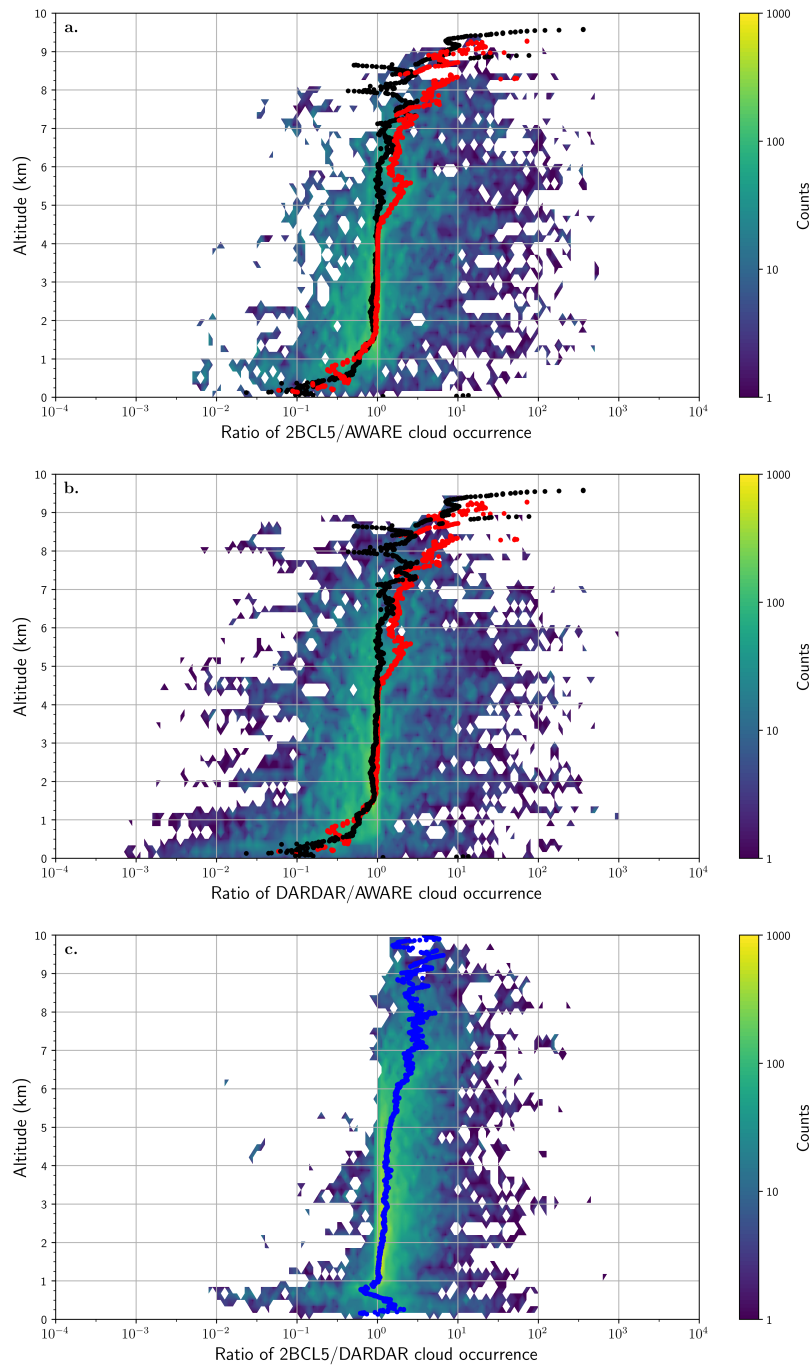


Figure 5. The ratio between satellite and ground-based cloud occurrence at different altitudes, for (a) 2BCL5/AWARE (b) DARDAR/AWARE and (c) 2BCL5/DARDAR. Both (a) and (b) display the medians for 2BCL5/AWARE (red) and DARDAR/AWARE (black) while the median for 2BCL5/DARDAR is shown on (c) in blue.

491 DARDAR starts to consistently underestimate cloud occurrence compared to AWARE
 492 below 1.5 km. The median drops to 0.37 at 0.5 km. This likely corresponds to limita-
 493 tions in DARDAR, which only observes 37% of cloud occurrence detected by AWARE
 494 at that altitude. As for the comparison with 2BCL5, the ratio between DARDAR and

495 AWARE cloud occurrence decreases towards the surface. Above 6 km the two datasets
496 also disagree, with AWARE underestimating cloud occurrence compared to the DAR-
497 DAR dataset. The median ratio fluctuates between 6 - 8 km, ranging from near even to
498 altitudes where AWARE has 37% of the DARDAR occurrences. At higher altitudes the
499 ratio changes rapidly as only a few profiles are available for the statistical analysis.

500 Figure 5c shows that DARDAR consistently underestimates cloud occurrence com-
501 pared to 2BCL5 above 1 km with only shows a few instances above 1 km where DAR-
502 DAR detects more cloud. This is possibly a result of the lower cloud occurrences in DAR-
503 DAR above 1 km (see Figure 2). Below 1 km there is clearly a wider range of ratios and
504 we might expect that DARDAR would show greater cloud occurrence below 1 km com-
505 pared to 2BCL5 based on Figure 4i. These ratios indicate that DARDAR may have greater
506 numbers of false cloud detections than 2BCL5.

507 3.5 Statistical evaluation of the 2BCL5, DARDAR and AWARE distri- 508 butions of cloud occurrence

509 The ratios of cloud occurrence rates clearly show distinct behaviours over differ-
510 ent altitude ranges. In order to quantify these differences, statistical tests are applied
511 to the distributions of cloud occurrence in 1 km altitude bins. Each of these regions are
512 examined using a t-test and a KolmogorovSmirnov (K-S) test. The t-test is used to an-
513alyze the differences in the means of cloud occurrence distributions between the 2BCL5
514 and AWARE and the DARDAR and AWARE datasets. The K-S test is used to com-
515pare whether the cloud occurrence distributions of 2BCL5 and AWARE or DARDAR
516 and AWARE are statistically distinct from one another. The t-test produces a t-statistic
517 (t), where a higher t-value indicates greater differences between the means of the dis-
518 tributions. The K-S test produces a K-S statistic (D), which evaluates the distance be-
519tween the two cumulative distribution functions with a higher D-value corresponding to
520 a greater distance. Both tests also produce a p-value, indicating the significance of the
521 test statistics. If the p-value is less than a predefined significance level (α), then the cor-
522 responding test statistics are considered statistically significant and the null hypothe-
523 sis can be rejected. Simply put if a p-value is above the significance level it implies the
524 satellites datasets agree with AWARE, while if it is below they are distinct from AWARE.
525 The significance level is chosen to be 5% and the results of the statistical tests are dis-
526 played in Figure 6.

527 Analysing the low level cloud between 0 and 1 km, the t-test and K-S test show
528 that both the means and distributions of 2BCL5 and DARDAR compared to AWARE
529 are statistically distinct. The largest t-values over this region are -7.0 between 2BCL5
530 and AWARE and -5.2 between DARDAR and AWARE. This indicates that the means
531 of these cloud occurrences are very different in both cases. The D-values in this region
532 are also large. Between 1 - 2 km, the K-S test indicates that the distributions of 2BCL5
533 and DARDAR are statistically distinct compared to AWARE, while the t-test shows that
534 the means cannot be considered different from AWARE. Between 2 - 5 km, 2BCL5 and
535 DARDAR match well with AWARE, as both tests show that the means and distribu-
536 tions are statistically similar. However, above 5 km the t-test shows drastically differ-
537 ent results for the 2BCL5 data. The results of the t-test show that the means of the dis-
538 tributions for the 2BCL5 and AWARE datasets cannot be considered to be drawn from
539 the same distribution, while the DARDAR and AWARE values continue to show that
540 the means are statistically similar. The K-S test continues to show show results above
541 the significance threshold for both 2BCL5 and DARDAR, although the 2BCL5 D-values
542 are clearly larger over this region. Given the relatively lower sensitivity of the AWARE
543 data over this region, these results should be interpreted cautiously.

544 Over the entire altitude range the DARDAR cloud occurrence distributions match
545 better to the AWARE data than the 2BCL5 based on both t and D values. The largest

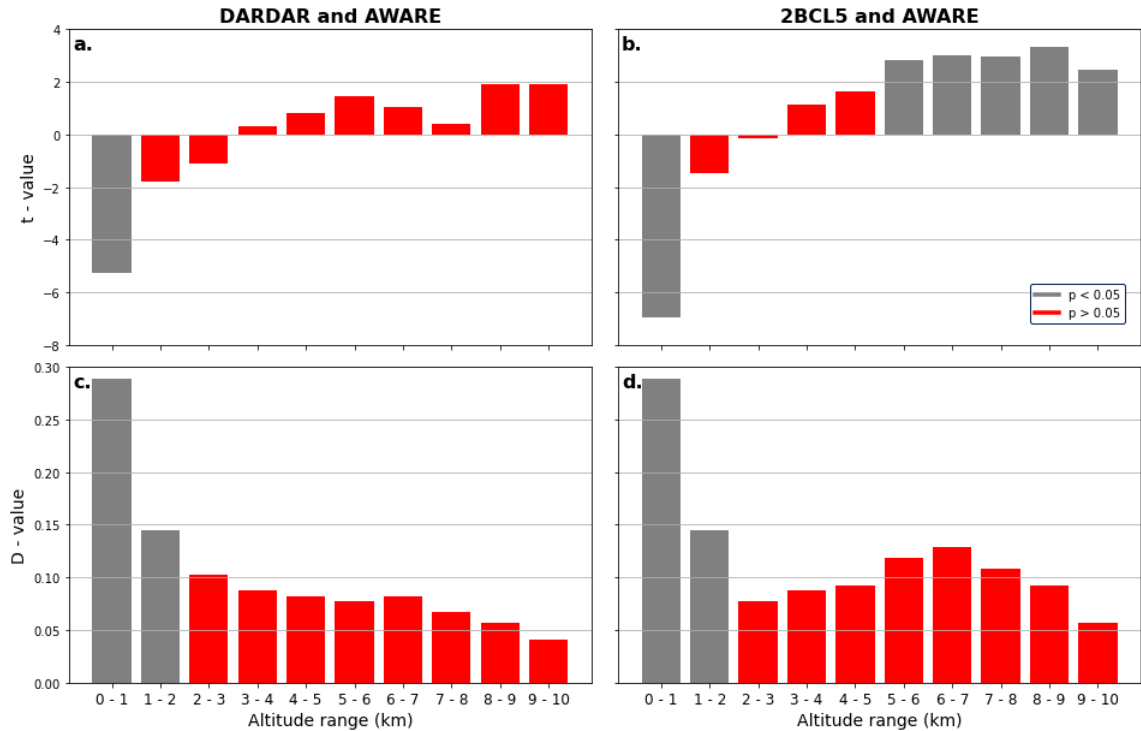


Figure 6. Results of the (a, b) t-test and (c, d) K-S test comparing the means and distributions of (a, c) DARDAR and AWARE and (b, d) 2BCL5 and AWARE. Red bars indicate where the p-value is greater than the significance level, $\alpha = 0.05$.

546 differences are seen above 5km where the t-tests consistently produce different results.
 547 This may seem to contradict the results that are shown in Figure 5, however this is due
 548 to differences in how these results should be interpreted. The statistics show that the
 549 underlying cloud occurrence distributions of DARDAR agree better with AWARE than
 550 2BCL5; However, the ratio analysis shows us that when specific cases are examined the
 551 2BCL5 data performs better. This implies that DARDAR might outperform 2BCL5 rel-
 552 ative to AWARE in the statistical aggregate, but when looking at specific times and
 553 locations 2BCL5 generally matches better.

554 3.6 Cloud occurrence as a function of temperature

555 To further compare the cloud phases in the 2BCL5, DARDAR, and AWARE datasets,
 556 cloud occurrence was derived as a function of temperature. Temperature information was
 557 taken from twice-daily measurements from radiosondes launched at McMurdo Station,
 558 as well as the ECMWF-AUX temperature data. Figure 7 shows the normalised occur-
 559 rence of cloud phase at each temperature for the three datasets examined, using both
 560 the ground-based and reanalysis temperature information.

561 Figure 7a shows 2BCL5 cloud occurrence identified relative to radiosonde temper-
 562 ature data. At temperatures above -8°C , supercooled water dominates, but its occur-
 563 rence quickly falls off as the proportions of mixed and ice phase cloud increases at lower
 564 temperatures. Ice phase clouds dominate occurrence at temperatures lower than -35°C .
 565 However, mixed phase clouds are identified at temperatures down to -60°C , which is clearly
 566 unphysical. This pattern matches well with Figure 7b, which uses the ECMWF-AUX
 567 measurements instead of the radiosondes. Thus, the unphysical classification can not be

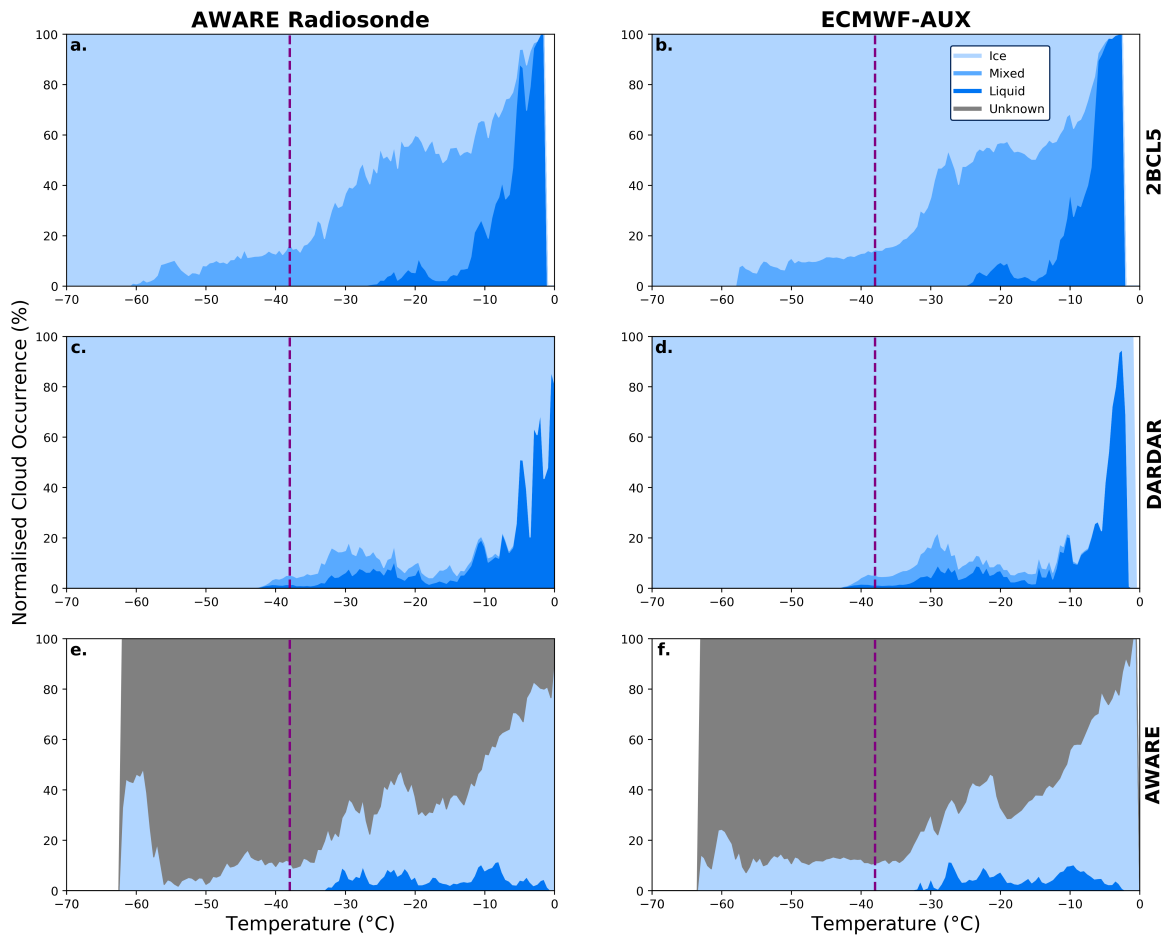


Figure 7. Normalised cloud occurrences from Figure 3 as a function of temperature for (a - b) 2BCL5 (c - d) DARDAR and (e - f) AWARE. 2BCL5 and DARDAR cloud occurrences are split into ice, mixed and liquid phases, and AWARE cloud occurrence into the ice, liquid and 'unknown' phase classes (see text for details). White space indicates where cloud is undetected and the dashed line indicates the edge of the homogeneous freezing regime at -38°C .

568 attributed to differences between the ECMWF-AUX data and the corresponding AWARE
 569 radiosonde measurements. Figures 7c and d display the DARDAR temperature based
 570 cloud occurrence. The DARDAR results identify that apart from a large presence of liq-
 571 uid phase clouds above -10°C , ice phase clouds dominate. However, small amounts of
 572 mixed and liquid phase cloud are present down to temperatures of -43°C , which again
 573 is unphysical. Once again, the ECMWF-AUX temperature output shows reasonable agree-
 574 ment with the ground-based temperature.

575 Figure 7e shows the AWARE cloud occurrence for different phases using the AWARE
 576 radiosonde measurements as the temperature reference. Most of the AWARE cloud de-
 577 tectations are associated with the 'unknown' phase, highlighting a clear limitation of the
 578 AWARE data. Liquid phase clouds are detected in relatively small fractions down to a
 579 temperature of approximately -35°C . Ice phase cloud occurrence (detected with the HSRL)
 580 is more common than liquid and unknown phases at the higher temperatures but falls
 581 off significantly at lower temperatures, because of increasingly large amounts of unknown
 582 phase cloud detections. A secondary peak of ice cloud at -60°C is partially associated

583 with polar stratospheric cloud detections in tropospheric cloud-free periods. This matches
584 observations in Figure 3 where the ability to classify phase falls off as altitude increases
585 (and conversely the temperature decreases), which is clearly due to the attenuation of
586 the HSRL signal by low-level cloud. Figure 7f again shows a good match between the
587 ECMWF-AUX and AWARE radiosonde temperature information, although the peak in
588 the ice phase cloud at -60°C is weaker.

589 Cloud phase data from AWARE matches well with the boundary of the homoge-
590 neous freezing regime at -38°C . There is some uncertainty in this result due to the ma-
591 jority of the clouds here being unclassified. The overall lack of liquid phase detections
592 in AWARE does suggest that some of the unknown phase detections are associated with
593 supercooled water. In both 2BCL5 and DARDAR, cloud measurements are found out-
594 side the physical limits defined by the homogeneous freezing threshold. For clouds clas-
595 sified as mixed phase by 2BCL5, 13.3% occur at temperatures below the -38°C isotherm
596 in the AWARE radiosonde measurements, and 13.8% for the ECMWF-AUX data prod-
597 uct. For the DARDAR dataset 1.1% of clouds classified as liquid phase and 5.7% of clouds
598 classified as mixed phase occur at temperatures below the -38°C isotherm for the AWARE
599 radiosonde measurements. When using ECMWF-AUX data as a reference 1.3% of clouds
600 classified as liquid phase and 6.6% of clouds classified as mixed phase occur add tem-
601 peratures below the -38°C isotherm. This coincident temperature analysis shows that
602 DARDAR also incorrectly classifies mixed phase cloud within the homogeneous freez-
603 ing regime, albeit to a smaller extent than 2BCL5.

604 4 Discussion

605 Figure 3 shows that cloud occurrence for all phases have maximum values between
606 1.5 and 3 km for both 2BCL5 and DARDAR. Below this level cloud occurrence falls off
607 rapidly with lesser cloud occurrence below 1 km for 2BCL5 and 0.5 km for DARDAR.
608 AWARE ground-based observations display a maximum in cloud occurrence at a slightly
609 lower altitude (between 1 and 2.5 km), but also show larger cloud occurrences at lower
610 levels. Above the maxima, AWARE cloud occurrence tends to fall off faster than the 2BCL5/DARDAR
611 data. As the lidar signal used within the AWARE dataset is often attenuated above 4
612 km, detection of high level clouds is likely underestimated. While the KAZR can still
613 detect many of these clouds, it struggles to detect high level cirrus with small optical depths
614 (Sassen & Khvorostyanov, 1998). Therefore neither 2BCL5, DARDAR or AWARE ap-
615 pears to be able to observe the complete vertical structure of clouds. Thus, to obtain the
616 full picture, a combination of ground-based and space-borne measurements are needed.
617 However, merging these datasets is not straight forward because of the large disparities
618 at nearly all altitudes. The underlying assumption that satellites have difficulties observ-
619 ing low level cloud due to lidar attenuation by thick cloud layers was investigated briefly.
620 In particular, we examined how the differences between cloud statistics in 2BCL5 and
621 AWARE changed for both single-layer and multi-layer clouds (not shown; See McEr-
622 lich (2020), section 5.3). We found that passes with single cloud layers have marginally
623 better agreement with AWARE than passes with multiple cloud layers. While this sup-
624 ports the assumption that attenuation of the lidar signal by multiple cloud layers is re-
625 ducing the quality of comparison with AWARE, even in cases where only a single cloud
626 layer is observed the low level satellite-based observations still struggle to match well
627 with AWARE. Thus, this topic will require further work in forthcoming studies.

628 The comparisons between the vertical profiles of cloud occurrence in AWARE, 2BCL5,
629 and DARDAR (see Figure 5) establish three distinct regions; a region where the satel-
630 lite likely underestimates cloud close to the ground, a region where the ground-based
631 instruments likely underestimate at higher altitudes, and a region of approximate agree-
632 ment in between. The statistical analysis in Figure 6 shows both 2BCL5 and DARDAR
633 are substantially different from AWARE at low altitudes. It might be expected that DAR-
634 DAR cloud occurrence would match better with the AWARE dataset than the 2BCL5

635 because DARDAR observes higher cloud occurrences below 1 km. However, this is not
636 the case, as the altitude at which the satellite datasets begin to deviate from AWARE
637 is essentially the same (see Figure 5). Thus, we conclude that even though DARDAR
638 observes more clouds below 1 km than 2BCL5, it does not appear to be detecting low-
639 level clouds more reliably than the 2BCL5 dataset. Instead, DARDAR appears to be de-
640 tecting false positives in the lidar/radar signals by incorrectly interpreting noise close
641 to the ground as clouds.

642 These results are generally consistent with conclusions from previous studies (e.g.,
643 Protat et al., 2014; Blanchard et al., 2014; Y. Liu et al., 2017; Alexander & Protat., 2018),
644 which show underestimations of satellite-based cloud observations compared to ground-
645 based observation (See McErlich (2020), section 5.1). For example, Alexander and Pro-
646 tat. (2018) found underestimation of DARDAR cloud observations by a factor of three
647 between 0.2 - 1 km compared with a ground-based lidar. However, their study only in-
648 cluded low level optically-thin single cloud layers where both the ground based lidar and
649 DARDAR masks could detect the cloud top and cloud base (lidar signal transmitted through
650 cloud top). Y. Liu et al. (2017) also found that space-borne observations, such as the
651 2B-GEOPROF-lidar dataset (Mace et al., 2009), begin to drop off significantly below
652 1 km similar to this study. In particular, they note that below 0.5 km satellite-based ob-
653 servations detect 2540% fewer clouds than observed by a ground-based lidar. One study
654 by Mioche et al. (2015) found that over the Svalbard region in the Arctic satellite ob-
655 servations overestimates cloud occurrence below 2 km compared to surface based micropulse
656 lidar observations. However, the authors associated this overestimation with the short
657 duration of their dataset. Previous work (e.g., Bodas-Salcedo et al., 2012; Schuddeboom
658 et al., 2018; Kuma et al., 2020) has shown climate models underestimate low-level cloud
659 compared to satellite datasets. Given that the satellite measurements in this paper are
660 shown to underestimate low-level cloud occurrence compared to AWARE observations,
661 the magnitude of these model errors could be larger than previously identified.

662 For the mid-altitude region, the median ratio (Figure 5) shows that 2BCL5 and AWARE
663 are in good agreement between 1.5 and 4.5 km and for the most part shows an equal amount
664 of cloud (within 10%). DARDAR shows a good level of agreement with AWARE between
665 1.5 and 6 km, extending further than 2BCL5, but the match is weaker (within 20%). This
666 match between DARDAR and AWARE extending to a greater altitude is likely because
667 both AWARE and DARDAR observe fewer clouds than 2BCL5 at these heights. The
668 results of the statistical tests (Figure 6) show that both DARDAR and AWARE and 2BCL5
669 and AWARE match well between 2 and 5 km, suggesting that the underlying cloud oc-
670 currence distributions are well captured in this region.

671 At altitudes greater than 6 km, the median ratio of cloud occurrence shows that
672 both DARDAR and 2BCL5 detect more clouds than AWARE, but this is probably due
673 to AWARE being unable to detect clouds rather than the satellite signals being dom-
674 inated by false positives. The ratio between the satellite and ground-based measurements
675 (Figure 5a/b) is variable at high altitudes and close to the ground because not all passes
676 can be compared at all heights. Figure 4c and Figure 4f show that above 7 km the com-
677 parisons between the two satellite datasets can only be made 10% of the time as the de-
678 tection frequency decreases. This suggests that the underestimation of AWARE at high
679 altitudes relative to 2BCL5 (Figure 5a) and DARDAR (Figure 5b) is potentially worse
680 than stated. Below 1 km a similar pattern is observed where the amount of detected cloud-
681 containing profiles that can be compared drops as the satellites are unable to observe
682 clouds detected by AWARE. The t-tests in Figure 6 show divergent results for 2BCL5
683 and DARDAR over this region, however due to the limitations with the AWARE dataset
684 these should be interpreted with caution.

685 Figure 7 shows that DARDAR and 2BCL5 observe mixed and liquid phase cloud
686 regions outside theoretical temperature thresholds using both the AWARE radiosonde
687 or ECMWF-AUX temperature data. However, the 2BCL5 data product classifies cloud

688 phase incorrectly more often than the DARDAR product despite the fact that both 2BCL5
689 and DARDAR use the same ECMWF-AUX temperature data. Differences in how 2BCL5/DARDAR
690 assign phase to their cloud detections must therefore explain why their phase determi-
691 nations are different. For 2BCL5, each cloud layer with a distinct top and bottom is as-
692 signed a single phase. DARDAR classifies each pixel in a cloud layer separately, so a cloud
693 layer identified by 2BCL5 might have multiple classifications given by DARDAR. This
694 could allow 2BCL5 to identify mixed phase at temperatures above the $-38\text{ }^{\circ}\text{C}$ isotherm
695 altitude. In addition, mixed phase clouds are defined by the 2BCL5 product as a com-
696 bination of ice and supercooled water existing in the cloud layer, resulting in the whole
697 cloud being classified as a mixed phase cloud. If a mixed phase cloud exists at the cloud
698 base where temperatures are between $0\text{ }^{\circ}\text{C}$ and $-38\text{ }^{\circ}\text{C}$, 2BCL5 would also assign a mixed
699 phase to the cloud top where temperatures are below $-38\text{ }^{\circ}\text{C}$ and mixed phase cloud will
700 not be present. Figure 1 identifies mixed phase cloud occurring at temperatures greater
701 than $0\text{ }^{\circ}\text{C}$ for 2BCL5. Similarly, the 2BCL5 phase classifications based on cloud layer
702 allows mixed phase cloud to exist at temperatures greater than $0\text{ }^{\circ}\text{C}$ if cloud layers with
703 a cloud base temperatures greater than $1\text{ }^{\circ}\text{C}$ and cloud top temperature smaller than
704 $-3\text{ }^{\circ}\text{C}$ are identified.

705 Due to a large proportion of the AWARE dataset clouds being classified as an un-
706 known phase, it becomes difficult to draw comparisons between cloud phases for the satellite-
707 and the ground-based datasets and to evaluate the reliability of liquid or mixed-phase
708 detections by the satellite retrievals within the heterogeneous freezing regime. 2BCL5
709 uses a process primarily driven by the temperature of the cloud top and cloud base, but
710 also uses a temperature dependent radar reflectivity (Z_e) threshold and an integrated
711 attenuated backscattering coefficient (see Zhang et al., 2010). This splits the cloud into
712 liquid, ice and mixed phase cloud containing a combination of ice and liquid. Contrast-
713 ingly, DARDAR uses the strength of the lidar backscatter signal to locate any attenu-
714 ating high backscatter layers. DARDAR then attempts to classify these layers based on
715 temperature, horizontal extent of layer, thickness, reflectivity, and altitude. The algo-
716 rithms used on the AWARE dataset use particulate backscatter cross-section and lin-
717 ear depolarisation ratio to split the lidar observations of cloud into liquid and ice cloud.
718 Due to attenuation of their lidar instrument, much of their cloud observations can not
719 be reliably classified and are instead classified as unknown (Silber et al., 2020). In or-
720 der to draw better comparisons between the phases, consistent processing algorithms with
721 high fidelity, which could simultaneously consider satellite and ground-based measure-
722 ment limitations, would be needed to be applied to the raw radar/lidar measurements
723 rather than trying to match separately processed products together. Another possibil-
724 ity is to use instrument simulators to help to interpret the different data relative to model
725 data (Kuma et al., 2020b).

726 5 Conclusions

727 In this study vertical profiles of cloud occurrence and cloud phase for the 2BCL5
728 and DARDAR satellite data products are compared to ground-based AWARE observa-
729 tions taken during 2016. An assessment of the global distributions of 2BCL5 and DAR-
730 DAR cloud occurrence found key differences between the two datasets quantification of
731 low-level clouds and cloud phase. These differences are greatest for low-level clouds over
732 high southern latitudes, providing a strong motivation for a detailed investigation of ver-
733 tical cloud occurrence using ground-based measurements from the AWARE campaign
734 over McMurdo Station in Antarctica.

735 Satellite observations for both 2BCL5 and AWARE show an underestimation of cloud
736 occurrence below 1.5 km compared to ground-based AWARE observations, with both
737 2BCL5 and DARDAR observing 37% of clouds detected at AWARE at an altitude of
738 0.5 km. Conversely, at altitudes greater than 6 km the AWARE dataset shows an un-
739 derestimation of cloud occurrence compared to the 2BCL5 and DARDAR datasets, likely

740 attributed to the attenuation of the HSRL signal by low-level clouds and lower KAZR
741 detectability at long ranges, where the radar volumes are significantly larger. In between
742 these altitude ranges, there was a good agreement between AWARE and the satellite-
743 based datasets.

744 Below 1 km DARDAR observes a greater cloud occurrence than 2BCL5, and rela-
745 tively lower occurrence at higher altitudes. Even though DARDAR observes more cloud
746 below 1 km than 2BCL5, when compared to coincident and contemporaneous AWARE
747 detections, it is not more reliable than the 2BCL5 dataset; DARDAR detects clouds that
748 are not detected in the AWARE dataset between 20–25% of the time below 1 km com-
749 pared to 10–15% for 2BCL5. This indicates that the higher DARDAR cloud occurrence
750 below 1 km is likely associated with false detections where DARDAR is likely incorrectly
751 classifying ground clutter or from the radar signal, or attenuated lidar retrievals, as cloud.

752 2BCL5 and DARDAR estimates of cloud phase were also found to deviate from phys-
753 ical constraints set by the temperatures at which a combination of ice and supercooled
754 water should exist. 2BCL5 shows 13.3% (13.8%) of mixed phase clouds occurring at tem-
755 peratures within the homogeneous freezing regime at temperatures below -38 °C, with
756 mixed-phase observations down to a temperature of -60 °C (-58 °C) in the case where
757 radiosonde (ECMWF-AUX) temperature data are used. DARDAR shows 5.7% (6.6%)
758 of mixed phase and 1.1% (1.3%) of liquid phase clouds within the homogeneous freez-
759 ing regime down to a temperature of -43 °C for radiosonde (ECMWF-AUX) data.

760 Overall, the results presented here emphasize the need for a combination of ground-
761 based and space-borne measurements to fully characterise cloud structure. This may be
762 particularly important over the Southern Ocean and Antarctica, given the large dispar-
763 ities observed in low-level cloud in this region and the tendency of climate models to un-
764 derestimate low-level cloud compared to satellite datasets.

765 While this study provides a comparison between satellite-based and ground-based
766 measurements of cloud occurrence, results presented in this paper may not be represen-
767 tative of the Southern Ocean as a whole. The analysis of how further ground-based datasets
768 compare with satellite retrievals in and around the Southern Ocean remains an impor-
769 tant area of work for future studies. Another aspect of this study that warrants further
770 analysis are the cloud occurrence measurements of 2BCL5 and DARDAR, which are shown
771 to have very significant differences of up to 30% over high southern latitudes. Given the
772 discrepancies displayed between 2BCL5, AWARE and DARDAR in how cloud phase is
773 determined, future work assessing what aspects of the phase determination algorithms
774 cause these differences is also required and will be the subject of future work using lower-
775 level data products.

776 Acknowledgments

777 The 2B-CLDCLASS-LIDAR and ECMWF-AUX products were obtained from the Cloud-
778 Sat Data Processing Center (<http://www.cloudsat.cira.colostate.edu/>). DARDAR data
779 products were downloaded from the ICARE Data and Service Center (<http://www.icare.univ->
780 [lille1.fr](http://www.archive.arm.gov)). The AWARE data used in this study are available in the ARM data archive
781 (<http://www.archive.arm.gov>). Data used to plot the figures is available at <https://zenodo.org/badge/latestdoi/29>
782 We would like to acknowledge funding from the Deep South National Science Challenge
783 which has partially supported this research. I.S. was supported by the DOE grants DE-
784 SC0017981. and DE-SC0018046.

785 References

786 Alexander, S. P., & Protat., A. (2018). Cloud properties observed from the surface
787 and by satellite at the northern edge of the southern ocean. *Journal of Geo-*
788 *physical Research: Atmospheres*, 123(1), 443-456. doi: 10.1002/2017jd026552

- 789 Blanchard, Y., Pelon, J., Eloranta, E. W., Moran, K. P., Delanoë, J., & Sze, G.
790 (2014). A synergistic analysis of cloud cover and vertical distribution from
791 a-train and ground-based sensors over the high arctic station eureka from 2006
792 to 2010. *Journal of Applied Meteorology and Climatology*, *53*(11), 2553-2570.
793 doi: 10.1175/jamc-d-14-0021.1
- 794 Bodas-Salcedo, A., Hill, P., Furtato, K., Williams, K., Field, P., Manners, J., &
795 Hyder, P. (2016). Large contribution of supercooled liquid clouds to the solar
796 radiation budget of the southern ocean. *Journal of Climate*, *29*(11), 4213-4228.
797 doi: 10.1175/jcli-d-15-0564.1
- 798 Bodas-Salcedo, A., Williams, K., Field, P., & Lock, A. (2012). The surface down-
799 welling solar radiation surplus over the southern ocean in the met office model:
800 The role of midlatitude cyclone clouds. *Journal of Climate*, *25*, 74677486. doi:
801 10.1175/jcli-d-11-00702.1
- 802 Bodas-Salcedo, A., Williams, K. D., Ringer, M. A., Beau, I., Cole, J. N. S.,
803 Dufresne, J. L., . . . Yokohata, T. (2014). Origins of the solar radiation bi-
804 ases over the southern ocean in cfmip2 models. *Journal of Climate*, *27*, 41-56.
805 doi: 10.1175/JCLI-D-13-00169.1
- 806 Ceccaldi, M., Delanoë, J., Hogan, R. J., Pounder, N. L., Protat, A., & Pelon,
807 J. (2013). From cloudsat-calipso to earthcare: Evolution of the dardar
808 cloud classification and its comparison to airborne radar-lidar observations.
809 *Journal of Geophysical Research: Atmospheres*, *118*(14), 7962-7981. doi:
810 10.1002/jgrd.50579
- 811 Ceppi, P., Hwang, Y.-T., Frierson, D. M., & Hartmann, D. L. (2012). Southern
812 hemisphere jet latitude biases in cmip5 models linked to shortwave cloud forc-
813 ing. *Geophysical Research Letters*, *39*(19). doi: 10.1029/2012GL053115
- 814 Cess, R. D. (1990). General circulation model intercomparisons for understand-
815 ing climate. long-term monitoring of the earth's radiation budget. *Journal of*
816 *Geophysical Research - Atmospheres*, *95*(D10), 16601-16615. doi: 10.1117/12
817 .21359
- 818 Chubb, T. H., Jensen, J. B., Siems, S. T., & Manton, M. J. (2013). In situ obser-
819 vations of supercooled liquid clouds over the southern ocean during the hiaper
820 pole-to-pole observation campaigns. *Geophysical Research Letters*, *40*(19),
821 5280-5285. doi: 10.1002/grl.50986
- 822 Coggins, J., A., M., & Jolly, B. (2014). Synoptic climatology of the ross ice shelf and
823 ross sea region of antarctica: k-means clustering and validation. *International*
824 *Journal of Climatology*, *34*(7), 2330-2348. doi: 10.1002/joc.3842
- 825 Delanoë, J., & Hogan, R. J. (2010). Combined cloudsat-calipso-modis retrievals of
826 the properties of ice clouds. *Journal of Geophysical Research*, *115*. doi: 10
827 .1029/2009jd012346
- 828 Eloranta, E. (2005). High spectral resolution lidar. in lidar: Range-resolved opti-
829 cal remote sensing of the atmosphere. *New York: Springer New York..* doi: 10
830 .1007/0-387-25101-4_5
- 831 Haynes, J. M., Jakob, C., Rossow, W. B., Tselioudis, G., & Brown, J. (2011). Major
832 characteristics of southern ocean cloud regimes and their effects on the energy
833 budget. *Journal of Climate*, *24*(19), 5061-5080. doi: 10.1175/2011jcli4052.1
- 834 Hu, Y., Winker, D., Vaughan, M., Lin, B., Omar, A., Trepte, C., & Flittner,
835 D. (2009). Calipso/caliop cloud phase discrimination algorithm. *Jour-
836 nal of Atmospheric and Oceanic Technology*, *26*(11), 2293-2309. doi:
837 10.1175/2009jtecha1280.1
- 838 Huang, Y., Siems, S., Manton, M., Protat, A., & Delanoë, J. (2012). A study on the
839 low-altitude clouds over the southern ocean using the dardar-mask. *Journal of*
840 *Geophysical Research: Atmospheres*, *117*. doi: 10.1029/2012JD017800.
- 841 Hwang, Y., & Frierson, D. (2013). Link between the double-intertropical con-
842 vergence zone problem and cloud biases over the southern ocean. *Pro-
843 ceedings of the National Academy of Sciences*, *110*(13), 4935-4940. doi:

- 10.1073/pnas.1213302110
- Hyder, P., Edwards, J., Allan, R., Hewitt, H., Bracegirdle, T., Gregory, J., ...
Belcher, E. (2018). Critical southern ocean climate model biases traced to
atmospheric model cloud errors. *Nature Communications*, 9(1), 3625. doi:
10.1038/s41467-018-05634-2
- Jolly, B., Kuma, P., McDonald, A., & Parsons, S. (2018). An analysis of the cloud
environment over the ross sea and ross ice shelf using cloudsat/calipso satellite
observations: The importance of synoptic forcing. *Atmospheric Chemistry and
Physics*, 18(13), 9723-9739. doi: 10.5194/acp-18-9723-2018
- Kay, J., Hillman, B., Klein, S., Zhang, Y., Medeiros, B., Pincus, R., ... T., A.
(2012). Exposing global cloud biases in the community atmosphere model
(cam) using satellite observations and their corresponding instrument simula-
tors. *Journal of Climate*, 25(15), 5190-5207. doi: 10.1175/jcli-d-11-00469.1
- Kay, J., Wall, C., Yettella, V., Medeiros, B., Hannay, C., Caldwell, P., & Bitz, C.
(2016). Global climate impacts of fixing the southern ocean shortwave radia-
tion bias in the community earth system model (cesm). *Journal of Climate*,
29(12), 4617-4636. doi: 10.1175/jcli-d-15-0358.1
- Kuma, P., McDonald, A., Morgenstern, O., Alexander, S., Cassano, J., Garrett, A.,
... Williams, J. (2020). Evaluation of southern ocean cloud in the hadgem3
general circulation model and merra-2 reanalysis using ship-based observations.
Atmospheric Chemistry and Physics Discussions, 20(11), 6607-6630. doi:
10.5194/acp-2019-201
- Kuma, P., McDonald, A. J., Morgenstern, O., Querel, R., Silber, I., & Flynn, C. J.
(2020b). Ground-based lidar processing and simulator framework for compar-
ing models and observations. *Geoscientific Model Development Discussions*,
2020, 1-45. Retrieved from <https://doi.org/10.5194/gmd-2020-25> (in
review) doi: 10.5194/gmd-2020-25
- Lamb, D., & Verlinde, J. (2011). Nucleation. In *Physics and chemistry of clouds*.
(p. 298-318). New York: Cambridge University Press.
- Listowski, C., Delanoë, J., Kirchgaessner, A., Lachlan-Cope, T., & King, J. (2018).
Antarctic clouds, supercooled liquid water and mixed-phase investigated with
dardar: Geographical and seasonal variations. *Atmospheric Chemistry and
Physics*, 19(10). doi: 10.5194/acp-19-6771-2019
- Liu, Y., Shupe, M. D., Wang, Z., & Mace, G. (2017). Cloud vertical distribution
from combined surface and space radar-lidar observations at two arctic atmo-
spheric observatories. *Atmospheric Chemistry and Physics*, 17(9), 5973-5989.
doi: 10.5194/acp-17-5973-2017
- Liu, Z. (2009). The calipso lidar cloud and aerosol discrimination: Version 2 al-
gorithm and initial assessment of performance. *Journal of Atmospheric and
Oceanic Technology*, 26(7), 1198-1213. doi: 10.1175/2009jtecha1229.1
- Lubin, D., Zhang, D., Silber, I., Scott, R. C., Kalogeras, P., Battaglia, A., ... Vo-
gelmann, A. M. (2020, 02). AWARE: The Atmospheric Radiation Measure-
ment (ARM) West Antarctic Radiation Experiment. *Bulletin of the Amer-
ican Meteorological Society*. Retrieved from [https://doi.org/10.1175/
BAMS-D-18-0278.1](https://doi.org/10.1175/BAMS-D-18-0278.1) doi: 10.1175/BAMS-D-18-0278.1
- Mace, G., Zhang, Q., Vaughan, M., Marchand, R., Stephens, G., Trepte, C., &
Winker, D. (2009). A description of hydrometeor layer occurrence statistics
derived from the first year of merged cloudsat and calipso data. *Journal of
Geophysical Research*, 114. doi: 10.1029/2007jd009755
- Marchand, R., Mace, G., Ackerman, T., & G., S. (2008). Hydrometeor detection
using cloudsat—an earth-orbiting 94-ghz cloud radar. *Journal of Atmospheric
and Oceanic Technology*, 25, 519-533. doi: 10.1175/2007JTECHA1006.1
- Marshall, J., & Plumb, R. A. (2008). *Atmosphere, ocean and climate dynamics: An
introductory text*. Elsevier.
- Mason, S., Fletcher, J. K., Haynes, J. M., Franklin, C., Protat, A., & Jakob, C.

- 899 (2015). A hybrid cloud regime methodology used to evaluate southern ocean
 900 cloud and shortwave radiation errors. *Journal of Climate*, 28, 6001-6018. doi:
 901 10.1175/JCLI-D-14-00846.1
- 902 Matus, A. V., & L'ecuyer, T. S. (2017). The role of cloud phase in earth's radiation
 903 budget. *Journal of Geophysical Research: Atmospheres*, 122(5), 2559-2578.
 904 doi: 10.1002/2016jd025951
- 905 McCoy, D., Hartmann, D., & Grosvenor, D. (2014). Observed southern ocean
 906 cloud properties and shortwave reflection. part i: Calculation of sw flux from
 907 observed cloud properties. *Journal of Climate*, 27(23), 8836-8857. doi:
 908 10.1175/jcli-d-14-00287.1
- 909 McErlich, C. (2020). Comparing satellite and ground based observations of cloud
 910 over the southern ocean. *University of Canterbury*. doi: [http://dx.doi.org/10](http://dx.doi.org/10.26021/946)
 911 [.26021/946](http://dx.doi.org/10.26021/946)
- 912 Mioche, G., Jourdan, O., Ceccaldi, M., & Delanoë, J. (2015). Variability of mixed-
 913 phase clouds in the arctic with a focus on the svalbard region: A study based
 914 on spaceborne active remote sensing. *Atmospheric Chemistry and Physics*,
 915 15(5), 2445-2461. doi: 10.5194/acp-15-2445-2015
- 916 Morrison, A. E., Siems, S. T., & Manton, M. J. (2011). A three-year climatology of
 917 cloud-top phase over the southern ocean and north pacific. *Journal of Climate*,
 918 24(9), 2405-2418. doi: 10.1175/2010jcli3842.1
- 919 Nayak, M. (2012). Cloudsat anomaly recovery and operational lessons learned.
 920 *SpaceOps 2012 Conference*. doi: 10.2514/6.2012-1295798.
- 921 Partain, P. (2007). *Cloudsat ecmwf-aux auxiliary data process description and*
 922 *interface control document*. Retrieved from [http://www.cloudsat.cira](http://www.cloudsat.cira.colostate.edu/sites/default/files/products/files/ECMWF-AUX_PDICD.P_R04.20070718.pdf)
 923 [.colostate.edu/sites/default/files/products/files/ECMWF-AUX_PDICD](http://www.cloudsat.cira.colostate.edu/sites/default/files/products/files/ECMWF-AUX_PDICD)
 924 [.P_R04.20070718.pdf](http://www.cloudsat.cira.colostate.edu/sites/default/files/products/files/ECMWF-AUX_PDICD)
- 925 Protat, A., Armstrong, A., Haeffelin, M., Morille, Y., Pelon, J., Delanoë, J., &
 926 Bouniol, D. (2006). Impact of conditional sampling and instrumental limita-
 927 tions on the statistics of cloud properties derived from cloud radar and lidar at
 928 sirta. *Geophysical Research Letters*, 33(11). doi: 10.1029/2005gl025340
- 929 Protat, A., Delanoë, J., O'Connor, E., & L'Ecuyer, T. (2010). The evaluation
 930 of cloudsat and calipso ice microphysical products using ground-based cloud
 931 radar and lidar observations. *Journal of Atmospheric and Oceanic Technology*,
 932 27(5), 793-810. doi: 10.1175/2009jtecha1397.1
- 933 Protat, A., Young, S. A., Mcfarlane, S. A., L'Ecuyer, T., Mace, G. G., Comstock,
 934 J. M., ... Delanoë, J. (2014). Reconciling ground-based and space-based
 935 estimates of the frequency of occurrence and radiative effect of clouds around
 936 darwin, australia. *Journal of Applied Meteorology and Climatology*, 53(2),
 937 456-478. doi: 10.1175/jamc-d-13-072.1
- 938 Rossow, W. B., & Schiffer, R. A. (1999). Advances in understanding clouds from is-
 939 ccp. *Bulletin of the American Meteorological Society*, 80(11), 2261-2287. doi:
 940 10.1175/1520-0477(1999)0802.0.co;2.
- 941 Salomonson, V., Barnes, W., Xiong, J., Kempler, S., & Masuoka, E. (2002). An
 942 overview of the earth observing system modis instrument and associated data
 943 systems performance. *IEEE International Geoscience and Remote Sensing*
 944 *Symposium..* doi: 10.1109/igarss.2002.1025812
- 945 Sassen, K. (1991). The polarization lidar technique for cloud research: A review and
 946 current assessment. *Bulletin of the American Meteorological Society*, 72(12),
 947 1848-1866. doi: 10.1175/1520-0477(1991)0722.0.co;2
- 948 Sassen, K., & Khvorostyanov, V. (1998). Radar probing of cirrus and contrails:
 949 Insights from 2d model simulations. *Geophysical Research Letters*, 25(7), 975-
 950 978. doi: 10.1029/98gl00731
- 951 Sassen, K., Wang, Z., & Liu, D. (2008). Global distribution of cirrus clouds
 952 from cloudsat/cloud-aerosol lidar and infrared pathfinder satellite observa-
 953 tions (calipso) measurements. *Journal of Geophysical Research*, 113. doi:

- 954 doi:10.1029/2008jd009972
- 955 Schuddeboom, A., McDonald, A. J., Morgenstern, O., Harvey, M., & Parsons, S.
956 (2018). Regional regime-based evaluation of present-day general circulation
957 model cloud simulations using self-organizing maps. *Journal of Geophysical*
958 *Research: Atmospheres*, *123*(8), 4259-4272. doi: 10.1002/2017jd028196
- 959 Schuddeboom, A., Varma, V., McDonald, A. J., Morgenstern, O., Harvey, M., Par-
960 sons, S., ... Furtado, K. (2019). Cluster-based evaluation of model compen-
961 sating errors: A case study of cloud radiative effect in the southern ocean.
962 *Geophysical Research Letters*, *46*(6), 3446-3453. doi: 10.1029/2018gl081686
- 963 Scott, R., & Lubin, D. (2014). Mixed-phase cloud radiative properties over ross
964 island, antarctica: The influence of various synoptic-scale atmospheric cir-
965 culation regimes. *Journal of Geophysical Research: Atmospheres*, *119*(11),
966 6702-6723. doi: doi:10.1002/2013jd021132
- 967 Silber, I., Verlinde, J., Cadetdu, M., Flynn, C. J., Vogelmann, A. M., & Eloranta,
968 E. W. (2019). Antarctic cloud macrophysical, thermodynamic phase, and
969 atmospheric inversion coupling properties at mcmurdo stationpart ii: Radiative
970 impact during different synoptic regimes. *Journal of Geophysical Research:*
971 *Atmospheres*, *124*(3), 1697-1719. doi: 10.1029/2018JD029471
- 972 Silber, I., Verlinde, J., Eloranta, E. W., & Cadetdu, M. (2018). Antarctic cloud
973 macrophysical, thermodynamic phase, and atmospheric inversion coupling
974 properties at mcmurdo station: I. principal data processing and climatology.
975 *Journal of Geophysical Research: Atmospheres*, *123*(11), 6099-6121. doi:
976 10.1029/2018jd028279
- 977 Silber, I., Verlinde, J., Wen, G., & Eloranta, E. W. (2020). Can embedded liq-
978 uid cloud layer volumes be classified in polar clouds using a single- frequency
979 zenith-pointing radar? *IEEE Geoscience and Remote Sensing Letters*, *17*(2),
980 222-226. doi: 10.1109/LGRS.2019.2918727
- 981 Stephens, G., Vane, D., Boain, R., Mace, G., Sassen, ., K, Wang, Z., ... Mitrescu,
982 C. (2002). The cloudsat mission and the a-train: A new dimension of space-
983 based observations of clouds and precipitation. *Bulletin of the American*
984 *Meteorological Society*, *83*(12), 1771-1790. doi: 10.1175/bams-83-12-1771
- 985 Stephens, G., Vane, D. G., Tanelli, S., Im, E., Durden, S., Rokey, M., ... Marchand,
986 R. (2008). Cloudsat mission: Performance and early science after the first
987 year of operation. *Journal of Geophysical Research: Atmospheres*, *113*. doi:
988 10.1029/2008jd009982
- 989 Tanelli, S., Durden, S. L., Im, E., Pak, K. S., Reinke, D. G., Partain, P., ... Marc-
990 hand, R. T. (2008). Cloudsat's cloud profiling radar after two years in orbit:
991 Performance, calibration, and processing. *IEEE Transactions on Geoscience*
992 *and Remote Sensing*, *46*(11), 3560-3573. doi: 10.1109/tgrs.2008.2002030
- 993 Trenberth, K. E., & Fasullo, J. T. (2010). Simulation of present-day and twenty-
994 first-century energy budgets of the southern oceans. *Journal of Climate*, *23*(2),
995 440-454. doi: 10.1175/2009jcli3152.1
- 996 Vergara-Temprado, J., Miltenberger, A., Furtado, K., Grosvenor, D., Shipway, B.,
997 Hill, A., ... Carslaw, K. (2018). Strong control of southern ocean cloud re-
998 flectivity by ice-nucleating particles. *Proceedings of the National Academy of*
999 *Sciences*, *115*(11), 2687-2692. doi: 10.1073/pnas.1721627115
- 1000 Wang, Z. (2019). *Cloudsat 2b-cldclass-lidar product process description and interface*
1001 *control document*. Retrieved from [http://www.cloudsat.cira.colostate](http://www.cloudsat.cira.colostate.edu/sites/default/files/products/files/2B-CLDCLASS-LIDAR_PDICD.P1_R05.rev0_.pdf)
1002 [.edu/sites/default/files/products/files/2B-CLDCLASS-LIDAR_PDICD.P1](http://www.cloudsat.cira.colostate.edu/sites/default/files/products/files/2B-CLDCLASS-LIDAR_PDICD.P1_R05.rev0_.pdf)
1003 [_R05.rev0_.pdf](http://www.cloudsat.cira.colostate.edu/sites/default/files/products/files/2B-CLDCLASS-LIDAR_PDICD.P1_R05.rev0_.pdf)
- 1004 Widener, K., Bharadwaj, N., & Johnson, K. (2012). Ka-band arm zenith radar
1005 (kazr) instrument handbook. *United States Department of Energy*. doi: doi:10
1006 .2172/1035855
- 1007 Winker, D., Hunt, W. H., & McGill, M. J. (2007). Initial performance assessment of
1008 caliop. *Geophysical Research Letters*, *34*(19). doi: 10.1029/2007gl030135

- 1009 Winker, D., Vaughan, M., Omar, A., Hu, Y., & Powell, K. (2009). Overview of the
1010 calipso mission and caliop data processing algorithms. *Journal of Atmospheric*
1011 *and Oceanic Technology*, 26(11), 2310-2323. doi: 10.1175/2009jtecha1281.1
1012 Zhang, D., Wang, Z., & Liu, D. (2010). A global view of midlevel liquid-layer
1013 topped stratiform cloud distribution and phase partition from calipso and
1014 cloudsat measurements. *Journal of Geophysical Research*, 115. doi:
1015 10.1029/2009jd012143

Accepted Article

